Measurement of the optical turbulence produced by a drone

Raúl Rodríguez García
Luis C. Alvarez Nuñez
Salvador Cuevas

Measurement of the optical turbulence produced by a drone

Raúl Rodríguez García,* Luis C. Alvarez Nuñez, and Salvador Cuevas
National Autonomous University of Mexico, Institute of Astronomy, Astronomical Instrumentation, Mexico City, Mexico

Abstract. At present, new approaches for the use of drones in high-precision optical applications are rising, especially with those known as multirotor. However, the optical turbulence effects generated by multirotor drones are not entirely understood. These optical effects can reduce the performance of the optical instruments that they transport. We present measurements of the wavefront deformation generated by the temperature fluctuations and the airflow of a drone's propulsion system. To do so, we used a single arm of a DJI S800 EVO Hexacopter (professional drone) and measured its operating temperature with a commercial infrared camera. The resulting temperature variation, between a switched-off propulsion system at room temperature and one running at its maximum performance, was 34.2°C. Later, we performed two different interferometric tests: Takeda's method and the phase-shifting technique, using a ZYGO interferometer. These tests show that the total deformation over an incident wavefront to the propeller airflow is lower than 0.074 λ PV and 0.007 λ RMS (HeNe laser, $\lambda = 633$ nm). We determine that the optical turbulence produced by a drone propulsion system is negligible.
© The Authors. Published by SPIE under a Creative Commons Attribution 4.0 Unported License. Distribution or reproduction of this work in whole or in part requires full attribution of the original publication, including its DOI. [DOI: 10.1117/1.OE.58.10.104107]

1 Introduction

The development of multirotor drones has been astounding, and today we can find them in a great variety of scientific applications.[1] The crucial point of this expansion has been the implementation of more robust and precise flight controllers, as well as the improvement of the battery technologies. These have increased drone's maneuverability (even automatically) and flight time, thereby easing their professional use for this sort of application.

Flight performance of multirotor drones has become more stable and accurate.[2] This development has inspired new applications involving the use of high precision optics, such as in astronomical instrumentation. Here, multirotor drones need to carry a light source that will use as a reference source for astronomical telescopes' applications. An example of these applications can be the maintenance of telescopes, optical telescope characterization,[3] or adaptive optics.[4] In our case, we want to determine the effects of optical turbulence produced by these types of drones in isothermal conditions. This characterization is necessary to validate the implementation of these devices as reference sources for the ground layer turbulence correction in astronomical observatories.[5] However, the understanding of this phenomenon can also be applied in the fields of aero-optics and free space optical communications.[6]

In optical instrumentation, there are several reasons why an optical system cannot reach its ideal performance. Sometimes inhere in their design and manufacturing parameters, and other times are resulting from external factors such as vibrations, temperature variations of their optomechanical components, and optical turbulence. The latter is produced by random variations in the refractive index of air due to changes in its density or temperature. These variations result in lower quality of the images obtained by the optical instruments. These variations are common and occur as a natural phenomenon in the atmosphere. This event is called atmospheric turbulence or seeing.

Seeing's effects depend on the interaction of air layers of different temperatures. This interaction produces optical turbulence in the form of randomly moving cells of air with different sizes and refraction indexes. When an incident wavefront refracts through those cells, it distorts. Then, this perturbed wavefront arrives on the input pupil of an optical system and blurs the formed image at the instrument focal plane. The strength of blur depends on the relative size of the cells, the wavelength, and the pupil diameter.

If the size of atmospheric cells is larger than the input pupil diameter, a perfect optical system will produce point spread function (PSF) images determined by the diffraction limit of the pupil. When the size of atmospheric cells is smaller than the pupil diameter, such that the number of encircled cells is bigger than three to four times, the PSF energy will be transferred from the central core to the diffraction rings at a rate of change determined by the velocity displacement of cells over the pupil.

This reasoning can be applied to the air flux produced by a drone propeller and its motor (propulsion system): the mixed layers circulating near a hot motor and the air layers propelled around it could generate optical turbulence. If the temperature difference among the mixed layers is large enough, the size of the cells could affect the wavefront transmitted from a light source placed on the drone.

To determine if a drone propulsion system produces optical turbulence, a first attempt would be numerical modeling of the air layers around the motor. This analysis would require knowing in advance the differences in temperature of the motor and the surrounding air, as well as the parameters of propeller and characteristics of air. We could use a

*Address all correspondence to Raúl Rodríguez García, E-mail: rrodriguez@astro.unam.mx

multiphysics numerical code based on finite element calculations. Nevertheless, the best approach is by measuring the optical turbulence produced by a drone propeller and its motor. That means to measure directly the wavefront distortions using instruments and techniques with enough optical sensitivity.

The purpose of this paper is to determine the optical turbulence produced by a drone's propulsion system. To this end, we conducted three different optical tests: a Schlieren imaging test and two interferometry tests (using the Takeda's method and the phase-shifting technique) under laboratory conditions. These optical tests also provide higher spatial resolution when compared to the Shack–Hartman wavefront analysis. In addition, we measured the temperature of the motor and the surrounding air using a thermal imaging infrared camera. This type of camera provides us the two-dimensional temperature distribution information in a large field of view (FoV), making it possible to observe not only the complete drone's propulsion system but also part of the testing lab.

Section 2 shows the measurements of the increase of temperature of the motor, running at its maximum power, using an infrared camera. Section 3 addresses the analysis of the distribution of turbulent airflow with Schlieren imaging test. Section 4 presents the development of an experiment using two different interferometric tests. This was because the propulsion system generated many vibrations, and we wanted to be sure about the obtained results from this experiment. Finally, we give a summary and our conclusions in Sec. 5.

2 Motor Temperature Variation

To evaluate the change in temperature of drone's propulsion system, we used a single arm of a DJI S800 EVO drone (see Fig. 1). Its features are described as follows:

- Motor: model: DJI-4114 400 Kv (Kv is a parameter used by motor manufacturers to characterize the electromechanical performance of their motors), max power: 500 W.
- Electronic speed controller (ESC): max current: 40 A, operating voltage: 22.2 V.
- Foldable propeller: engineering plastic, size: 15×5.2 in.

Usually, the motors of a multirotor drone receive operating signals directly from the drone's flight controller. For the tests and to run one motor independently, we developed an electronic control board to adjust the speed of the propulsion system as required. With this control board, we also

Fig. 1 DJI S800 EVO propulsion system.

monitored the motor electrical parameters (voltage, current, and power) during the experiment.

As mentioned already, it is necessary to have differences in temperature within an air flow to induce a distortion on an incident wavefront. We determined the change of temperature of the drone's propulsion system using an FLIR E8 infrared camera. This camera has the following features: IR resolution: 320×240 pixels, FoV: 45 deg $\times$ 34 deg, and in each pixel a thermal sensitivity: 0.06°C.[7] These characteristics allow us to analyze the thermal behavior of the engine and the surrounding air. For example, at one and a half meters away from the target, we observe an equivalent area of 1.5 m $\times$ 1 m, enough to frame the 55 cm of the length of drone's propulsion system, and part of the laboratory.

First, using the infrared camera, we measured the temperature of the drone's propulsion system at room temperature when the motor was switched off. Then, we made another measurement after 5 min of motor operation at its maximum speed.

Figure 2 shows two thermal images taken with the infrared camera. The value highlighted on the top left corner of both images represents the temperature of the central spot (spotmeter).[8] Both thermal images have a uniform colored background around the propulsion system due to the laboratory has a controlled temperature. This condition ensures that the surrounding air has the same temperature. At the moment of conducting the tests, the value of the laboratory thermostat was of 20°C. This value differs slightly from the value obtained with the thermal camera.

It is not unusual to find that, both in addition to the motor and in a separate form, electronic devices used to control and power the propulsion system are other sources of heat. However, in the case of our experiment, these elements are included in the base of the motor (see DJI S-800 User's manual[9]), so the obtained measurements incorporate the total amount of the generated heat. The difference in temperature by the comparison of the spotmeter value from both thermal images is 34.2°C (see Fig. 2) [The lateral bar in both images (values at the right top and bottom corners) show the temperature scale. This bar is auto-adjusting to obtain the best contrast of the image.].

Besides, we can compare the obtained value with the performance of a propulsion system with similar specs on the T-motors company website. We found the data-sheet of the motor model MN4014 400 Kv with a carbon fiber propeller 15×5. This motor reaches an operating temperature of 46°C after 10 min of use at its maximum power.[10] This temperature value is consistent with our measurements.

For all subsequent tests, we used the same procedure for the drone's propulsion system operation: we run its motor for 5 min at its maximum speed and then reduce the velocity by half to do the measurements. In this way, we ensure that the increase in temperature of the propulsion system was similar for all the tests. Likewise, for all the tests, the temperature of the laboratory was controlled to 20°C.

3 Distribution of Turbulent Flow

To better understand the distribution of the heated air flux produced by the propulsion system, we performed a Schlieren test. This kind of test has been widely used to study air flux-related problems.[11] For this test, we used the largest mirror available in our laboratory (60 cm diameter), since the area
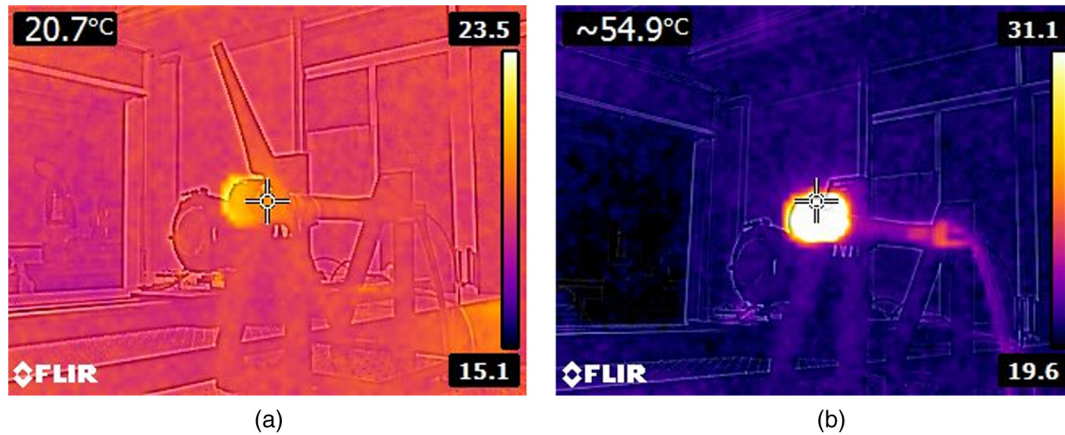
Fig. 2 The increase in temperature of the motor. (a) The thermal image when the motor was off and (b) the thermal image after 5 min of operating the motor at its maximum speed.

covered by the rotating propeller is 40 cm in diameter. In this qualitative test, we ran the motor to its maximum speed for about 5 min, and then we reduced this speed by half to perceive the optical effects of turbulence.

3.1 Schlieren Test Setup

The Schlieren test is a widely known optical technique that makes visible the refractive index fluctuations in transparent media such as the air. At present, we can find several Schlieren configurations and applications for the metrology of several phenomena, including turbulent flows.[12] Moreover, the implementation of this technique has become easier due to the use of modern technologies such as digital cameras and LED lighting.[13]

We implemented the Schlieren test with a double pass coincident setup with a spherical mirror 60 cm of diameter and 4.4 m of focal distance (see Fig. 3). The propulsion system was supported by a metal structure. This structure was placed so that the motor was in front of the mirror at a distance of 50 cm. At this distance, we positioned the propulsion system above and below to the mirror image formed on the camera's CCD (Schlieren test area). This configuration allows the air flux to cross through the total test area. The
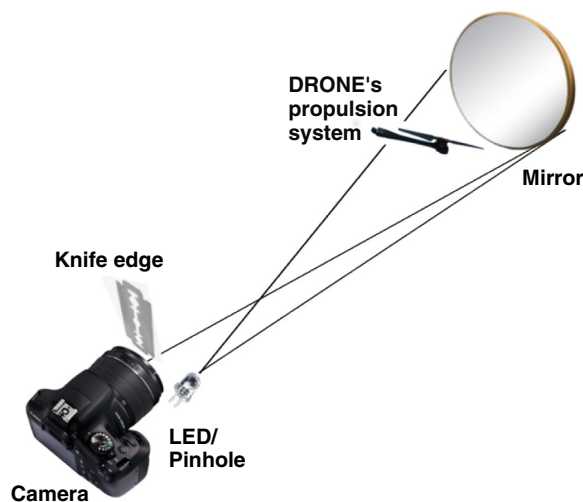
light source was a circular pinhole 1 mm in diameter illuminated by a white LED (1-W high power). We acquired the images using a Canon T3i camera with a 22.3×14.9 mm CMOS detector and a 50-mm objective lens focused on the motor.

3.2 Results of the Schlieren Test

First, we placed the propulsion system above the test area. In this configuration, the downward air produced by the propellers crossed the entire mirror. Nevertheless, we did not detect any variation (turbulence) in the Schlieren image.

Next, we placed the propulsion system below the test area, under the assumption that the heated air was probably going to move upward. Again, we did not detect any turbulence after running the motor for 5 min. Nonetheless, only when we switched off the motor after conduct this test, the camera registered fluctuations produced by the ascending heated air due to heat exchange with the motor housing and its windings (see Fig. 4).

It was not possible to see optical turbulence using the Schlieren test. Therefore, it was not possible to detect its distribution. These preliminary results led us to infer that the turbulence must be close to the motor. Hence, for the interferometric tests, we decided to place the propulsion system as close as possible to the light beam (see Fig. 5).

4 Wavefront Measurements

This section describes the experiment that we implemented to estimate the optical turbulence produced by the drone's propulsion system. We proposed to use interferometric methods since they are the best ways to detect and quantitatively measure the smallest variations (smaller than $\lambda/10$) of wavefront respect to a reference surface.

To measure wavefront distortions, we did two interferometric tests with the aim to compare and confirm the obtained results. For both tests, we used a 6 in. Fizeau interferometer (ZYGO interferometer) with a high-performance transmission flat ($\lambda/20$). It should be mentioned that the interferometer of our optical laboratory is certified by the National Institute of Standards and Technology (NIST). The first interferometric test was the Fourier interferometric fringe pattern analysis, also known in optics as the Takeda's method.[14] The second test was using the phase-shifting technique made

Fig. 3 Setup of the Schlieren test performed to get information on the distribution of the optical turbulent flow.
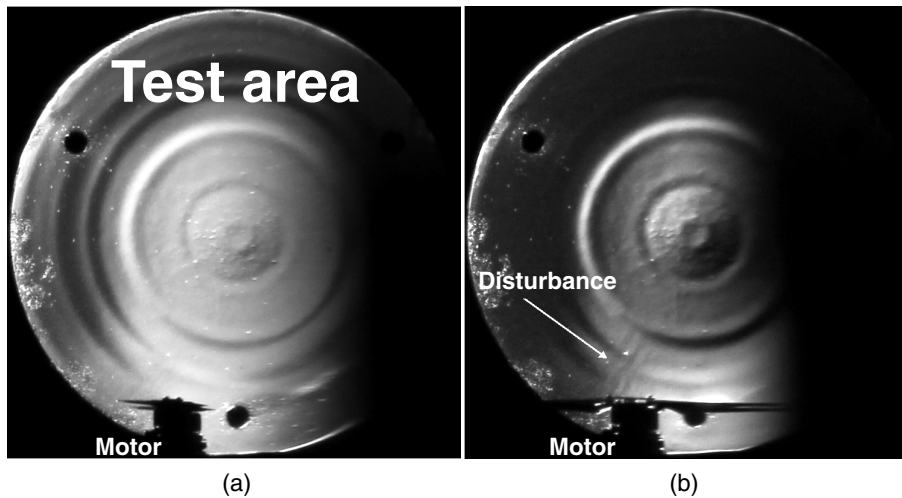
Fig. 4 Schlieren test with (a) an operating motor and (b) the motor turned off. (b) The turbulence produced by the heat of the stopped motor after running for several minutes. The circular patterns are due to defects in the polishing of the mirror.
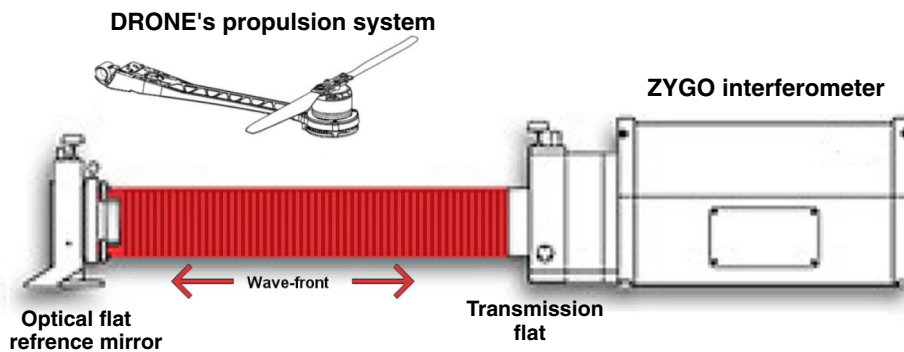
Fig. 5 Interferometric experiment layout.

directly by the ZYGO software. We used MATLAB® to process and display the phase maps obtained in both tests. The phases are in units of λ referenced to a He-Ne laser ($\lambda = 633$ nm). Besides, we present the results by means of the root mean square (RMS) and peak to valley (PV) of the wavefront surface with the same units.

In both tests, we ran the motor to its maximum speed for 5 min. Its electrical parameters were: voltage of 21.3 V, current of 19.79 A, and 418 W of power (the maximum specified operating power is 500 W). Next, we reduced the motor speed by half (20.9 V, 5.4 A, and 113 W). Then, we made eight measurements during the next 5 min. This procedure simulates the flight of a drone until it reaches a required operating height, and then maintaining a static flight (hover mode) to perform some task.

4.1 Experiment Setup

In the experiment setup, an external 4 in. flat reference mirror ($\lambda/12$ PV) reflected the light beam from the interferometer by the same optical path. This arrangement allows us to have a reference wavefront. Figure 5 shows a layout of the performed experiment.

With this experimental configuration, any small temperature variation distorts the wavefront in a double pass. This configuration doubles the sensitivity of the experiment. We

placed the drone propulsion system at a distance of 35 cm from the light beam with the rotation axis of the propeller perpendicular to the optical beam direction. The purpose of this was that the heated air crosses the beam of light (see Fig. 6).
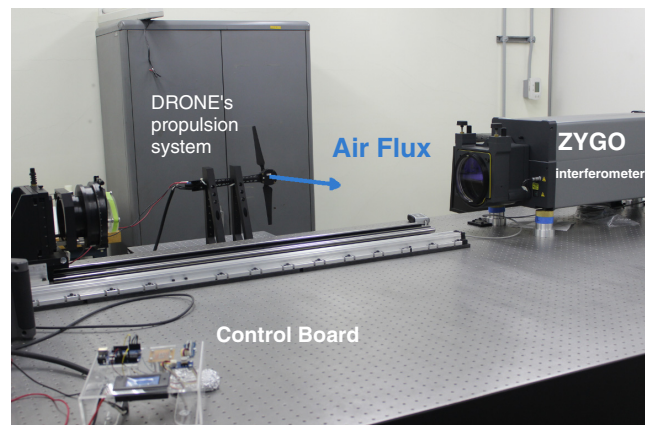
Fig. 6 Experiment setup. The propulsion system was isolated from the optical table, and we operated it by the control board. The propeller was placed laterally directing the hot air flow perpendicular to the interferometer axis (light beam).
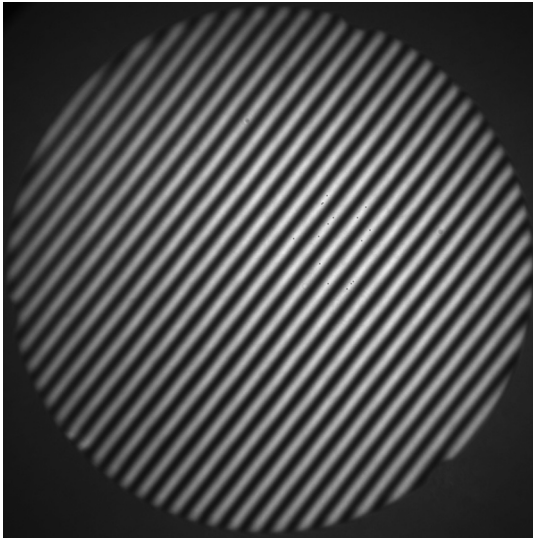
Fig. 7 Interferogram of the reference flat mirror with a small tilt.

4.2 Analysis with the Takeda's Method

The first interferometric test was the Takeda's method due to the fact that the normal operation of the drone's propulsion system produces vibrations. The Takeda's method is very effective in the presence of small mechanical vibrations as it uses only one image from the interference fringe pattern or interferogram to obtain the phase-map information. The interferogram freezes the instantaneous characteristics of the wavefront, including the turbulence effects at this moment.

It is important to have a considerable number of fringes so that the algorithm can work correctly.[15] We modified the number of obtained fringes by small adjustments in the tilt of the external flat reference mirror. Figure 7 shows an example of a fringe pattern obtained for the Takeda's method test.

We implemented the Takeda's method analysis in MATLAB®, to get the phase-maps from the interferograms. It is worth mentioning that we needed to calibrate our software to get the actual values of PV and RMS from the phase-maps' measurements.

We did the calibration of our software by comparing one of its postprocessed phase-maps with one obtained by a standard measurement of ZYGO interferometer (phase-shifting). Both of them were from the flat reference mirror under the same conditions. In the calibration process, we performed the measurements without the influence of the propulsion system. It is important to highlight that the measurement for calibration must be done in controlled room temperature to avoid the effects of temperature variations such as stress and deformation of the optomechanical systems and the optical turbulence of the air.

Figure 8 shows the phase-maps of the flat reference mirror obtained by the two previously described measurements over the same test area. Figure 8(a) shows the obtained phase-map by ZYGO software. And Fig. 8(b) shows the resulting phase-map of the processing with Takeda's method software. The colors represent the value of the phase in waves (He–Ne laser). Here, the wavefront errors after the calibration were the same, $0.077 \, \lambda$ PV and $0.013 \, \lambda$ RMS.

For each measurement, we subtracted the phase-map obtained without the influence of the propulsion system (the calibration phase-map) to isolate the turbulence effects in the tests. This subtracted phase-map includes the errors of the flat reference mirror. Therefore, we can consider it as the instrumental error.

We ran the propulsion system for 5 min at its maximum speed and then we reduced this speed by half. Then, we took eight interferograms over the next 5 min to be postprocessed.

Figure 9 shows the results achieved by the implemented software. The min and max values of RMS were 0.005 and $0.006 \, \lambda$, respectively. The mean PV of all the events was $0.067 \, \lambda$ ($\lambda/15$) and the mean RMS is $0.056 \, \lambda$, equivalent to a Strehl ratio of 0.998 (using Marechal's formula).

(a)

(b)
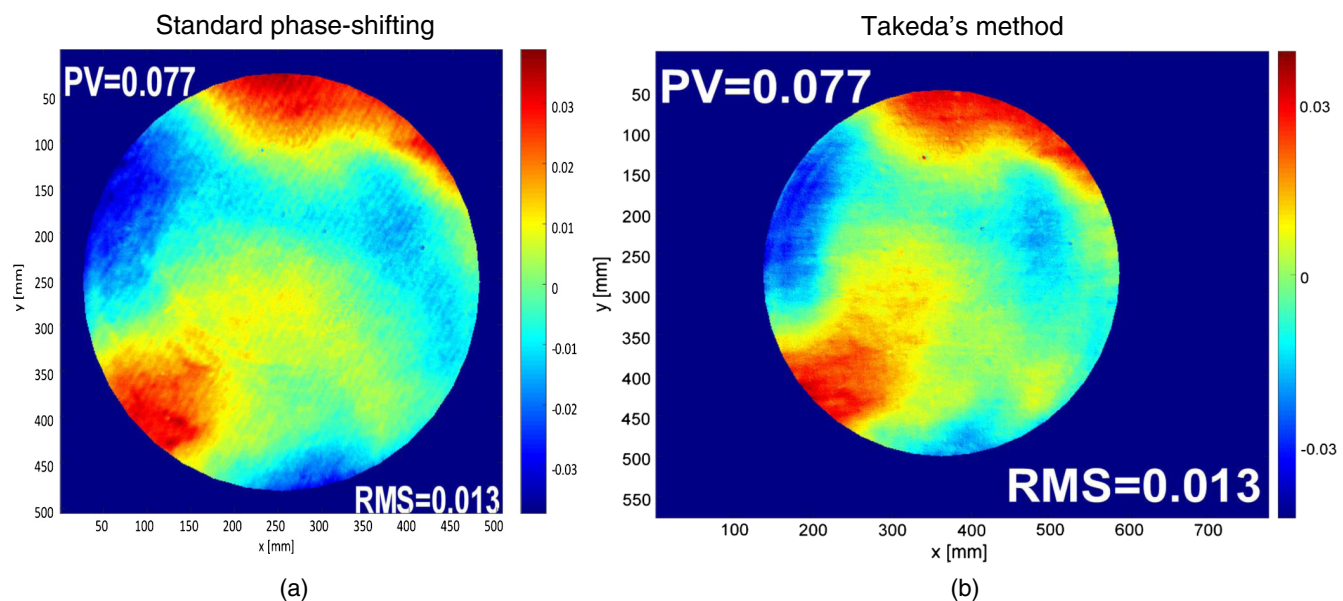
Fig. 8 Comparison of the phase-maps of the flat reference mirror used to calibrate the developed software. (a) A standard ZYGO measurement (phase-shifting) and (b) a measurement with the Takeda's method software after adjusting the values of PV and RMS.

Takeda's method results
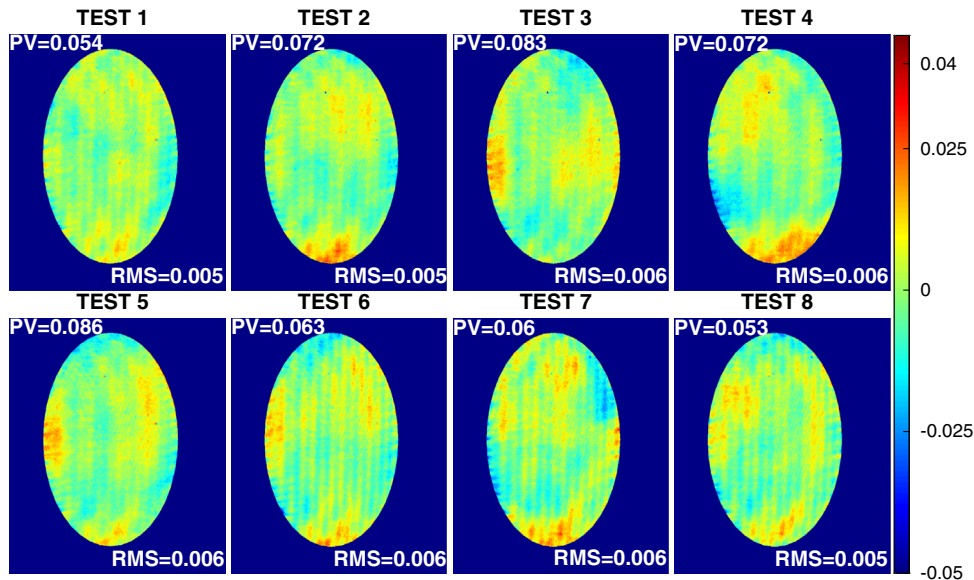
Fig. 9 Experiment phase-maps obtained with the Takeda's method software.

The obtained results using the Takeda's method show random variations between each phase-map. However, the obtained PV values are lower than $\lambda/13$, so we can consider it negligible.

4.3 Analysis with the Phase-Shifting Technique

Complementary to this work, we verified the results obtained by the Takeda's method. To do this, we performed direct interferometric measurements with the ZYGO instrument. However, even though the motor was isolated from the optical table, the propulsion system produced vibrations by the ejected air from the propeller to the optical table. We made standard phase-shifting measurements, but the resulted phase-maps were distorted. Figure 10 shows the distortion of the obtained phase-map. Here, the wavefront errors were of 0.237 λ PV and 0.032 λ RMS.
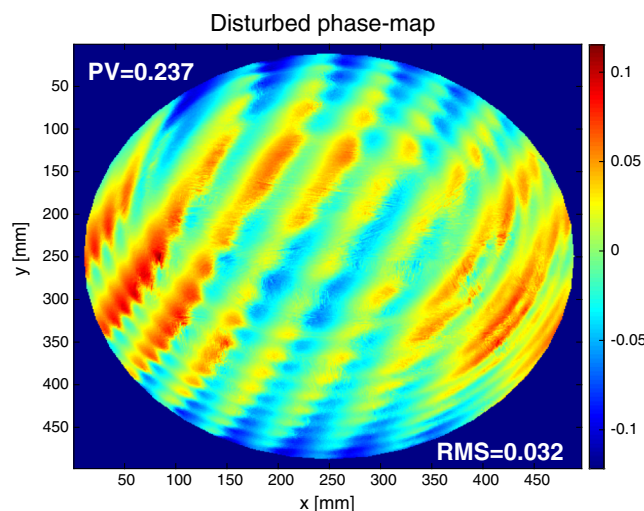
Fig. 10 Phase-map showing the disturbance produced by the vibration of the optical table.

In order to eliminate the effects of vibrations, we modified the acquisition time parameter of the interferometer camera from 2000 μs (default value) to 5 μs. However, when conducting various measurements on the reference flat mirror, we found variations in the resulting phase-maps, even without the influence of the propulsion system. We attributed these variations to the reduction of the signal-to-noise ratio resulting from the reduction of the exposure time.

Similarly to the previous test, we isolated the effects of turbulence subtracting the instrumental error from each of the measurements. In this case, the instrumental error was the average of 10 short exposure phase-maps made with the ZYGO interferometer software. Then, this error was subtracted from each measurement using the ZYGO software.

In Fig. 11, we show the results of the phase-shifting technique measurements. In this case, we have a mean PV of 0.046 λ ($\lambda/21$) and min/max RMS values of 0.007 and 0.009 λ, respectively, with a mean RMS of 0.007 λ, equivalent to a Strehl ratio of 0.998.

The short exposure phase-shifting results show random variations between each phase-map, too. The values of RMS and PV obtained have a magnitude comparable to those obtained with the Takeda's method software. This test confirms that the effects of turbulence are negligible.

5 Summary and Conclusion

We measured the temperature of a drone propulsion system (motor, propeller, and electronics) using an infrared camera. We obtained a difference of 34.2°C after running the propulsion system at its maximum speed for 5 min.

We conducted a Schlieren test to determine the distribution of turbulence flow. In this test, we did not see the optical turbulence. However, we observed optical disturbances produced by the heat of the motor when we switched-off the propulsion system after running the test.

We also conducted two interferometric tests using a ZYGO interferometer: one performed with the postprocessing of interferograms using a Takeda's method software

Phase-shifting results
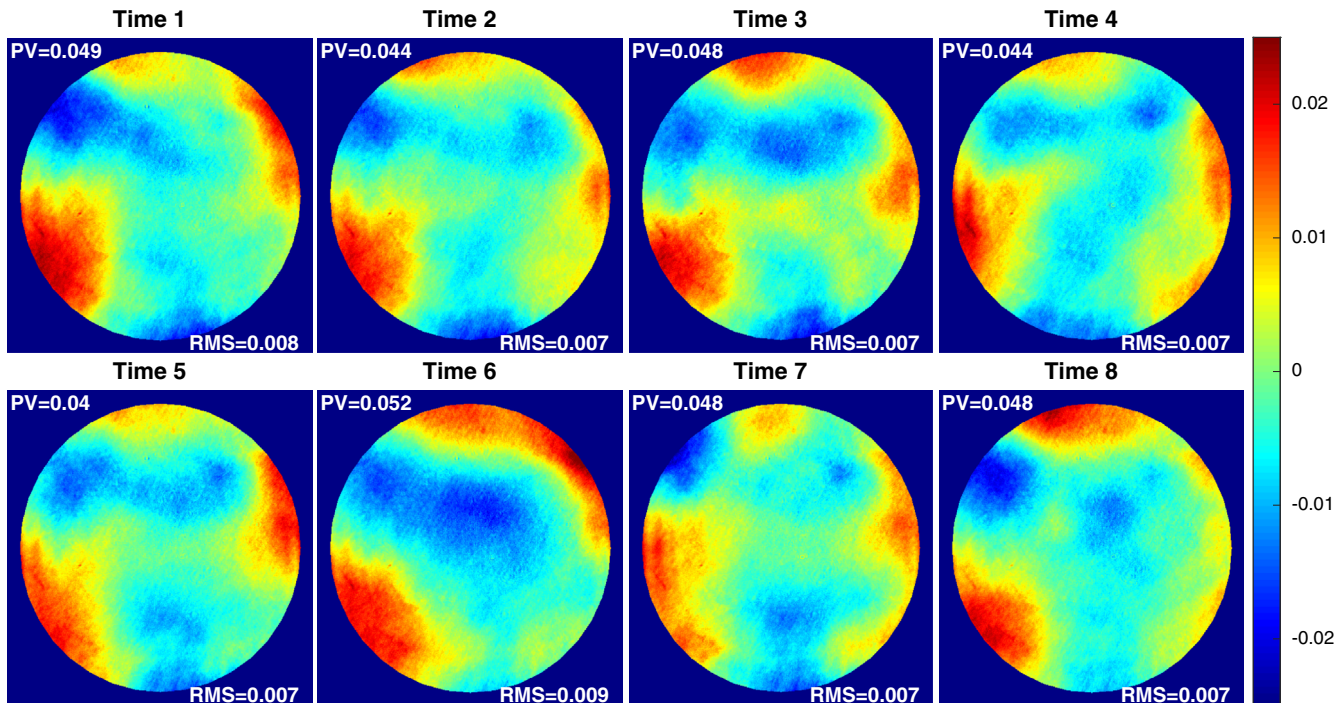
Fig. 11 Experiment phase-maps obtained with the phase-shifting technique with a short exposure time.

and another using the phase shifting technique with a modified acquisition time.

The results of all the tests show random variations between each phase-map. The wavefront errors are under the instrumental error (PV value of $\lambda/13$). The equivalent Strehl ratio obtained from RMS values of the short exposure phase-shifting test and the Takeda's method test is 0.98.

As a result of our experiment, we can affirm that the propulsion system does not produce significant optical turbulence. Therefore, drones can be used in high-precision optical applications.

References

1. C. Kyrkou et al., "Drones: augmenting our quality of life," *IEEE Potentials* **38**(1), 30–36 (2019).
2. F. Benassi et al., "Testing accuracy and repeatability of UAV blocks oriented with GNSS-supported aerial triangulation," *Remote Sens.* **9**(2), 172 (2017).
3. F. Biondi et al., "Unmanned aerial vehicles in astronomy," *Proc. SPIE* **9912**, 991210 (2016).
4. A. G. Basden et al., "Artificial guide stars for adaptive optics using unmanned aerial vehicles," *Mon. Not. R. Astron. Soc.* **477**(2), 2209–2219 (2018).
5. R. Rodríguez García and S. Cuevas, "Implementation of MUAV as reference source for glao systems," *Exp. Astron.* (2019).
6. M. T. Dabiri, S. M. S. Sadough, and M. A. Khalighi, "Channel modeling and parameter optimization for hovering UAV-based free-space optical links," *IEEE J. Sel. Areas Commun.* **36**, 2104–2113 (2018).
7. FLIR, "FLIR E8" support information"," https://www.flir.com/support/products/e8#Resources (accessed 2019-09-03).
8. FLIR, "FLIR EX series user manual," https://www.flir.com/globalassets/imported-assets/document/t559828_en-us_a4.pdf (accessed: 2019-09-03).
9. DJI, "Spreading wings S800 EVO user manual," http://dl.djicdn.com/downloads/s800evo/en/S800_EVO_User_Manual_v1.10_en.pdf (accessed 2018-10-11).
10. T-Motor, "MN4014 KV400" specifications tab"," http://store-en.tmotor.com/goods.php?id=348 (accessed 2018-12-02).
11. G. S. Settles and E. B. Hackett, "Full-scale Schlieren flow visualization," in *Intl. Symp. Flow Visual.*, pp. 2–13 (1995).
12. G. S. Settles, *Schlieren and Shadowgraph Techniques: Visualizing Phenomena in Transport Media*, Springer-Verlag, Berlin, Heidelberg (2001).
13. G. S. Settles and M. J. Hargather, "A review of recent developments in Schlieren and shadowgraph techniques," *Meas. Sci. Technol.* **28**, 042001 (2017).
14. M. Takeda, H. Ina, and S. Kobayashi, "Fourier-transform method of fringe-pattern analysis for computer-based topography and interferometry," *J. Opt. Soc. Am.* **72**(1), 156 (1982).
15. W. W. Macy, "Two-dimensional fringe-pattern analysis," *Appl. Opt.* **22**, 3898–3901 (1983).

Raúl Rodríguez García received his BE in mechatronics and MSEE in instrumentation from the Universidad Nacional Autónoma de México (UNAM). He has developed optical instruments applied to astronomical instrumentation at Instituto de Astronomía (IA), UNAM. He worked on the manufacture of the optical components of the FRIDA instrument, a collaboration project between the IA-UNAM and the Instituto de Astrofísica de Canarias. He is currently studying innovative applications of drones for astronomical instrumentation.

Luis C. Alvarez Nuñez studied electronics engineering at the Technological Institute of Durango, Mexico; later, he completed his masters and PhD studies at Centro de Investigaciones en Óptica in Guanajuato, Mexico, in the area of optical engineering. He participated in the first ISCAI2009 Advanced Instrumentation school in the Canary Islands, Spain, working on the M5 mirror control system for the E-ELT at the company NTE-SENER, in Barcelona, Spain.

He is currently working in the development of optical instruments at IA, UNAM.

Salvador Cuevas received his BSc degree in physics from UNAM, an optical engineer's degree from Ecole Supèrieure d'Optique/ Institut d'Optique Graduate School, France, and his PhD from the Université Paris-Sud, France. He has been involved on astronomical instrumentation projects for 30 years in Mexico, where he has strongly contributed to form an astronomical instrumentation engineering group at IA, UNAM. He is the author of more than 20 refereed papers and 90 SPIE technical papers and has been MSc and PhD advisor of over 20 students.